5-7-2022

Electron Traps in Ag-doped $Li_2B_4O_7$ Crystals: The role of Ag Interstitial Ions

Timothy D. Gustafson
Air Force Institute of Technology

Brant E. Kananen
Air Force Institute of Technology

Nancy C. Giles
Air Force Institute of Technology

Brian C. Holloway
Air Force Institute of Technology

Volodymyr T. Adamiv
Institute of Physical Optics - Lviv, Ukraine

See next page for additional authors

Recommended Citation

T. D. Gustafson, B. E. Kananen, N. C. Giles, B. C. Holloway, V. T. Adamiv, I. M. Teslyuk, Ya. V. Burak, L. E. Halliburton; Electron traps in Ag-doped Li2B4O7 crystals: The role of Ag interstitial ions. Journal of Applied Physics 7 May 2022; 131 (17): 175106. https://doi.org/10.1063/5.0088122

Journal of Applied Physics

RESEARCH ARTICLE | MAY 06 2022

Electron traps in Ag-doped $Li_2B_4O_7$ crystals: The role of Ag interstitial ions

T. D. Gustafson ; B. E. Kananen; N. C. Giles ; B. C. Holloway; V. T. Adamiv ; I. M. Teslyuk ; Ya. V. Burak ; L. E. Halliburton

Journal of Applied Physics 131, 175106 (2022)
https://doi.org/10.1063/5.0088122

Journal of Applied Physics ARTICLE scitation.org/journal/jap

Electron traps in Ag-doped $Li_2B_4O_7$ crystals: The role of Ag interstitial ions

Cite as: J. Appl. Phys. **131**, 175106 (2022); doi: 10.1063/5.0088122
Submitted: 13 February 2022 · Accepted: 19 April 2022 ·
Published Online: 6 May 2022

T. D. Gustafson,[1,a)] B. E. Kananen,[1] N. C. Giles,[1] B. C. Holloway,[1] V. T. Adamiv,[2] I. M. Teslyuk,[2] Ya. V. Burak,[2] and L. E. Halliburton[3,b)]

AFFILIATIONS

[1]Department of Engineering Physics, Air Force Institute of Technology, Wright-Patterson Air Force Base, Ohio 45433, USA
[2]Department of Optical Materials, Vlokh Institute of Physical Optics, 23 Drahomanov Street, Lviv 79005, Ukraine
[3]Department of Physics and Astronomy, West Virginia University, Morgantown, West Virginia 26506, USA

[a)]**Email:** Timothy.Gustafson@protonmail.com
[b)]**Author to whom correspondence should be addressed:** Larry.Halliburton@mail.wvu.edu

ABSTRACT

Electron paramagnetic resonance (EPR) is used to establish models for electron traps in Ag-doped lithium tetraborate ($Li_2B_4O_7$) crystals. When exposed at room temperature to ionizing radiation, electrons are trapped at interstitial Ag^+ ions and holes are trapped at Ag^+ ions on Li^+ sites. The trapped electrons occupy a $5s^1$ orbital on the interstitial Ag ions (some of the unpaired spin density is also on neighboring ions). Three EPR spectra are assigned to electrons trapped at interstitial Ag ions. Their g values are near 1.99 and they have resolved hyperfine structure from ^{107}Ag and ^{109}Ag nuclei. The spectrum representing the largest concentration of trapped electrons has the unpaired spin shared by the interstitial Ag ion and an adjacent boron ion at its regular lattice site. A ^{10}B enriched crystal verifies this assignment and an analysis of spin-Hamiltonian parameters yields information about the Ag and B orbitals occupied by the unpaired spin. The second spectrum has the unpaired spin shared equally by two Ag ions, one at an interstitial site and the other at an adjacent Li site. The third spectrum has a large Ag hyperfine interaction and a weak Li interaction. Optical absorption bands associated with the trapped electrons are observed between 225 and 500 nm. Thermal release of electrons from these traps is responsible for a prominent thermoluminescence peak near 150 °C, whereas optical release of the electrons at room temperature produces intense optically stimulated luminescence. Radiative recombination occurs at Ag^{2+} ions with emission peaking near 270 nm.

I. INTRODUCTION

Recent studies have shown that lithium tetraborate ($Li_2B_4O_7$) crystals doped with Ag^+ ions are a sensitive, near tissue equivalent, radiation detector material.[1–5] They are presently being considered for use as thermoluminescence (TL) and optically stimulated luminescence (OSL) dosimeters.[6–8] The excellent performance of the Ag-doped $Li_2B_4O_7$ crystals in these applications is a direct result of (1) an efficient radiative electron–hole recombination process and (2) the ability of Ag^+ ($4d^{10}$) ions to serve as both hole traps and electron traps.[9–16] In crystals doped with Ag during growth and in crystals diffused with Ag after growth, the Ag^+ ions are present at two locations. They replace Li^+ ions and they occupy interstitial sites. During an exposure at room temperature to ionizing radiation, the Ag^+ ions at Li^+ sites trap holes and the interstitial Ag^+ ions trap electrons. This forms Ag^{2+} ($4d^9$) ions and Ag^0 ($5s^1$) atoms, respectively. When the trapped electrons are released from interstitial Ag^0 atoms during subsequent heating or optical stimulation, they recombine with holes at Ag^{2+} ions and produce easily monitored luminescence near 270 nm. A detailed understanding of the electronic structure and the thermal stability of these electron and hole traps will help optimize the performance of Ag-doped $Li_2B_4O_7$ radiation detectors. Also, knowing the identities, properties, and relative concentrations of the participating electron and hole traps will be especially useful when modeling the kinetics of TL glow curves and OSL decay curves.[17–22]

The radiation-induced holes trapped by Ag^+ ions occupying Li^+ sites in the $Li_2B_4O_7$ crystals have been extensively studied.[3,10,14,15] When trapping a hole, the Ag^+ ions become Ag^{2+} ions with an unpaired spin in the 4d shell and, thus, can be directly

observed with electron paramagnetic resonance (EPR). Positive g shifts and resolved hyperfine lines from ^{107}Ag and ^{109}Ag nuclei make their EPR signals easy to identify.[10,14] Two similar, yet distinct, Ag^{2+} spectra have been observed in $Li_2B_4O_7$ crystals. One spectrum represents the Ag^{2+} ions on Li^+ sites with no nearby defects and the other spectrum is from Ag^{2+} ions that have a nearby Li vacancy.[3,14] These defects are referred to as isolated and perturbed Ag^{2+} centers, respectively. Only the isolated Ag^{2+} ions serve as recombination sites in OSL,[3] whereas both the isolated and perturbed Ag^{2+} ions participate in the TL.[10]

Less is known about the trapped-electron centers involving interstitial Ag^+ ions. After trapping an electron, the Ag interstitials have an unpaired spin in the 5s shell and can be monitored with EPR. Until now, only one electron trap has been reported for Ag-doped $Li_2B_4O_7$ crystals. An early investigation assigned a 16-line EPR spectrum to trapped electrons in irradiated Ag-doped $Li_2B_4O_7$ crystals.[10] The proposed model was an electron trapped by an interstitial Ag^+ ion with an overlap of the unpaired spin onto an adjacent ion with an I = 3/2 nuclear spin (both ^{7}Li and ^{11}B nuclei have I = 3/2 and the data available at that time could not distinguish between the two). In the present paper, a crystal enriched with ^{10}B is used to establish a more complete model for this initially observed trapped-electron spectrum (the ^{10}B nuclei have an I = 3 nuclear spin). We confirm the interstitial nature of the defect and show conclusively that the interacting neighboring ion is boron and not lithium. This interstitial Ag electron trap is labeled Center Ag–B, where B denotes the interacting boron. A recent comprehensive density functional theory (DFT) study by Santos *et al.*[23] predicted that one boron ion would participate in the primary Ag interstitial electron trap, a result in agreement with our experimental findings.

The present paper also greatly expands our understanding of electron traps in Ag-doped $Li_2B_4O_7$ crystals by providing a complete analysis of a second EPR spectrum that has an interstitial Ag ion sharing the unpaired spin with an adjacent Ag ion on a Li^+ site. This second defect is labeled Center Ag–Ag. It is expected to play a significant role in $Li_2B_4O_7$ crystals with large Ag concentrations. In addition to the Ag–B and Ag–Ag electron traps, another less intense electron trap involving an interstitial Ag ion is observed. This third defect (which we identify as Center Ag–Li) has a large hyperfine interaction with an interstitial Ag ion and a much smaller hyperfine interaction with an I = 3/2 nucleus. Our ^{10}B enriched crystal demonstrates that the participating I = 3/2 nucleus in this third defect is not ^{11}B. This leaves a ^{7}Li nucleus as the only choice.

Broad optical absorption bands in the visible and ultraviolet accompany the formation of the trapped-electron EPR spectra. These absorption bands have large oscillator strengths and represent transitions to excited states of the trapped-electron centers. Production conditions, thermal stabilities, and bleaching effects are reported for the EPR and optical absorption spectra. An intense TL peak near 150 °C is directly related to the thermal release of the trapped electrons.

II. EXPERIMENTAL DETAILS

Two large $Li_2B_4O_7$ crystals were grown by the Czochralski method at the Vlokh Institute of Physical Optics (Lviv, Ukraine). During growth, a congruent melt was exposed to air while contained in a Pt crucible. The growth axis was [001] and pulling and rotation velocities did not exceed 0.3 mm/h and 10 revolutions/min. One boule was doped with Ag during growth (all isotopes were present in their natural abundances). The concentration of Ag in this boule is estimated from the starting materials to be 0.02 at.%. The second boule was not doped with Ag but was enriched with ^{10}B during growth. The ^{10}B isotope is approximately 97% abundant in this second boule. Samples for the EPR and optical experiments were cut from the larger boules. In a post-growth treatment, Ag^+ ions were diffused into one EPR-sized sample cut from the ^{10}B enriched boule. The crystal was wrapped in Ag foil (0.25 mm thick) and then held near 870 °C for 10 h in a flowing nitrogen atmosphere. In addition to the Ag ions, our as-grown $Li_2B_4O_7$ crystals contain singly ionized lithium vacancies (V_{Li}^-) and doubly ionized oxygen vacancies (V_O^{2+}).[24] The lithium vacancies provide charge compensation for the Ag^+ interstitials and oxygen vacancies.

The EPR spectra were taken with a Bruker EMX spectrometer operating near 9.4 GHz. An Oxford helium-gas flow system controlled the temperature of the sample for spectra taken below room temperature and a Bruker NMR teslameter was used to measure the magnetic fields. A Cr-doped MgO crystal provided small corrections for the difference in the magnetic field between the positions of the sample and the teslameter probe (Cr^{3+} ions in MgO have an isotropic g value of 1.9800). The relative concentrations of trapped electrons were determined by comparing the intensities of the highest-field EPR line in each spectrum (this intensity was multiplied by the number and degeneracies of the remaining lines and adjusted for slightly different line widths). Uncertainties resulting from this process are estimated to be approximately 5%. Absolute concentrations of the EPR-active defects were not determined.

The crystals were irradiated with x rays from a Varian OEG-76H-Rh tube operating at 60 kV and 30 mA (irradiation times varied from 3–5 min). Before an irradiation, the crystal was reset by briefly heating to 500 °C (this returned the electron and hole traps to their as-grown non-paramagnetic charge states). A Harshaw 3500 TL reader, with a neutral density filter (2 OD) placed between the sample and the photomultiplier tube, was used to collect TL glow curves. No additional filters were used. All thermal anneals were done in the Harshaw reader by selecting the appropriate T_{stop} value. The heating rate for all anneals and TL curves was 1 °C/s. Optical absorption spectra were taken with a Cary 5000 spectrophotometer.

Lithium tetraborate crystals are tetragonal (space group $I4_1cd$ and point group $4mm$) with 104 atoms (eight formula units) in a unit cell.[25–28] The room-temperature lattice constants are $a = 9.475$ Å and $c = 10.283$ Å. This structure has two inequivalent boron sites and four inequivalent oxygen sites. All lithium sites are equivalent. A ball-and-stick representation of the $Li_2B_4O_7$ lattice, such as shown in Ref. 3, is easily produced by inserting the crystallographic results[25–28] into VESTA (a 3D visualization program that generates structural models).[29,30] The repeating $(B_4O_9)^{6-}$ anionic group within the crystal has two boron ions (labeled B1) with three oxygen neighbors and two boron ions (labeled B2) with four oxygen neighbors. Each oxygen ion has two boron neighbors. Each lithium ion is surrounded by five oxygen ions (O1, O2, O3, O3, and O4). The first four of these O^{2-} ions are close to the Li^+ ion (their average Li–O separation distance is 2.064 Å at room

TABLE I. Nuclear spins, natural abundances, and nuclear magnetic moments of nuclei responsible for resolved hyperfine structure in irradiated Ag-doped $Li_2B_4O_7$ crystals. The magnetic moments are expressed in units of the nuclear magneton β_n. This information is taken from Refs. 33 and 34.

Nucleus	Nuclear spin	Natural abundance (%)	Nuclear magnetic moment (μ)
^{7}Li	I = 3/2	92.41	+3.256 46β_n
^{10}B	I = 3	19.9	+1.800 64β_n
^{11}B	I = 3/2	80.1	+2.688 65β_n
^{107}Ag	I = 1/2	51.84	−0.113 68β_n
^{109}Ag	I = 1/2	48.16	−0.130 69β_n

temperature) and the O4 ion is farther away (the Li–O4 separation distance is 2.592 Å).[26]

When considering models for Ag-related electron traps in the $Li_2B_4O_7$ crystal, it is helpful to compare the effective radii of Ag ions (Ag^{2+}, Ag^{+}, and Ag^{0}) with the effective radii of the constituent B^{3+} and Li^{+} ions.[31] All three Ag ions are much too large to replace a B^{3+} ion. In the strongly covalent $(BO_3)^{3-}$ and $(BO_4)^{5-}$ units, the effective radius of the boron ion is only about 0.11 Å, whereas the effective radii of Ag^{+} and Ag^{2+} ions in fourfold coordination are 1.00 and 0.79 Å, respectively. The situation is different for the Li^{+} sites. In sixfold coordination, the effective radii of Ag^{+} and Ag^{2+} ions are 1.15 and 0.94 Å, respectively, and the effective radius of Li^{+} ions is 0.76 Å. Thus, the Ag^{+} and Ag^{2+} ions can replace a Li^{+} ion with only a small amount of outward displacement of the surrounding oxygen ions and perhaps a small shift of the Ag ion off the center of the Li site.[23] In contrast, the outer 5s electron makes the radius of the Ag^{0} atoms approximately 1.44 Å. This is significantly larger than the radius of a Li^{+} ion and suggests that radiation-induced Ag^{0} atoms will occupy interstitial positions.

III. EPR RESULTS

Irradiating a $Li_2B_4O_7$ crystal at room temperature with x rays produces large concentrations of "free" electrons and holes. Many of these electrons and holes immediately recombine, but a significant portion is trapped at pre-existing intrinsic defects and impurities. The primary focus of the present paper is the electrons trapped at interstitial Ag^{+} ions. In this section of the paper, we describe three Ag-related EPR spectra that are formed during or after an irradiation with x rays. Resolved hyperfine interactions with magnetic nuclei (I > 0) are the dominant characteristics of these spectra. EPR studies often use hyperfine information to identify and construct models of paramagnetic point defects.[32] In the present investigation, interactions with ^{107}Ag, ^{109}Ag, ^{10}B, ^{11}B, and ^{7}Li nuclei provide the critical information that allows models to be established. The nuclear spins, natural abundances, and magnetic moments for these isotopes are listed in Table I.[33,34]

A. Silver-boron trapped electron (Center Ag–B)

Figure 1(a) shows the primary trapped-electron EPR spectrum produced in a Ag-doped $Li_2B_4O_7$ crystal during an irradiation at room temperature with x rays.[10] This crystal was doped with Ag during growth, and all isotopes are present in their natural abundances. The spectrum in Fig. 1(a) was taken at 40 K with the magnetic field along the [001] direction. Although the spectrum is easily seen at room temperature, the lines sharpen slightly at a lower

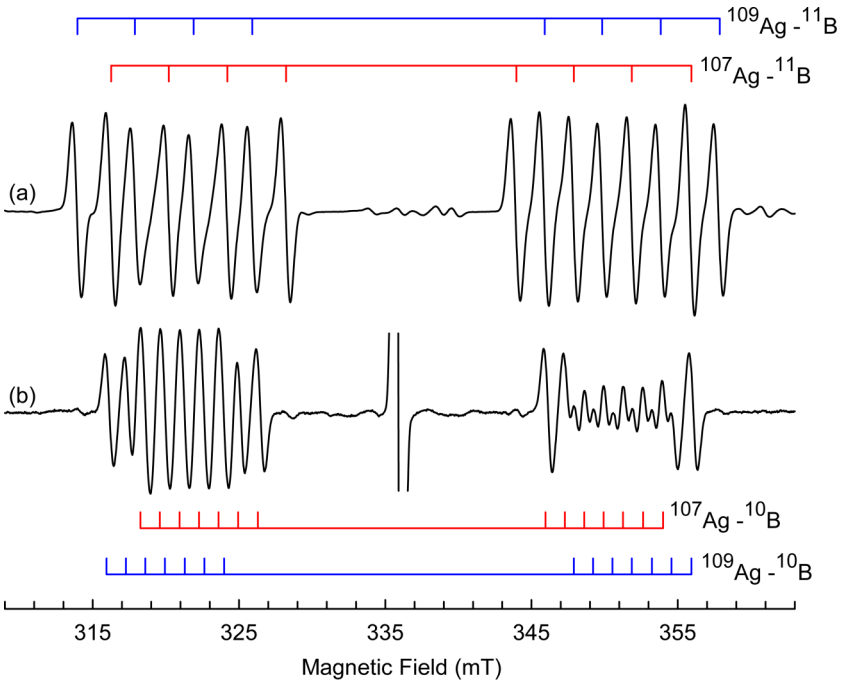

FIG. 1. EPR spectra from Center Ag–B. These spectra were taken at 40 K after an x-ray irradiation at room temperature. The magnetic field was along the [001] direction, and the microwave frequency was 9.393 GHz. Labels to the right of the stick diagrams identify the participating nuclei. (a) Spectrum from a crystal with natural abundances of ^{10}B and ^{11}B. (b) Spectrum from a crystal 97% enriched with ^{10}B. The line in the center of the lower spectrum is tentatively assigned to Ag nanoparticles.

temperature. The S = 1/2 spectrum in Fig. 1(a) consists of two well-separated sets of eight lines caused by hyperfine interactions with ^{107}Ag and ^{109}Ag nuclei (both I = 1/2) at one Ag site and an I = 3/2 nucleus at a neighboring site. If only hyperfine from Ag nuclei was present, there would be a total of four lines (instead of 16). Large hyperfine interactions with the ^{107}Ag and ^{109}Ag nuclei give two lines in the higher field region and two lines in the lower field region. As shown by the stick diagrams above the spectrum, each of the four lines from the Ag nuclei is further split into four additional lines by the hyperfine interaction with a neighboring I = 3/2 nucleus having a high natural abundance, thus giving the observed 16 lines. Because they are intrinsic constituents of the $Li_2B_4O_7$ crystals, the nucleus responsible for this latter interaction was suggested in an earlier study[10] to be either ^{7}Li (92.4% abundant) or ^{11}B (80.1% abundant). Both ^{7}Li and ^{11}B have I = 3/2 nuclear spins.

Evidence to clearly establish the identity of the nucleus causing the sets of four lines in Fig. 1(a) is obtained in our present study by diffusing Ag^+ ions into a ^{10}B enriched $Li_2B_4O_7$ crystal. After irradiating the enriched crystal at room temperature with x rays, the EPR spectrum in Fig. 1(b) was acquired at 40 K with the magnetic field along the [001] direction. [Note: The line near g = 2.00 in the center of the spectrum in Fig. 1(b) is tentatively assigned to Ag nanoparticles[35,36] formed during the in-diffusion of the Ag ions. It is given no further consideration in the present paper.] The spectra in Figs. 1(a) and 1(b) were obtained with identical spectrometer settings and, thus, can be directly compared. Lines in the high- and low-field regions of these spectra represent the same defect, i.e., an electron trapped at an interstitial Ag ion with significant overlap of the wavefunction onto a neighboring ion. There are, however, important differences: the spectrum from the ^{10}B enriched crystal has more lines and the spacing between lines is smaller.

These differences in the two spectra in Fig. 1 are readily explained if the unpaired spin on the Ag interstitial ion is interacting with a ^{11}B nucleus in Fig. 1(a) and with a ^{10}B nucleus in Fig. 1(b). As indicated by stick diagrams below the spectrum in Fig. 1(b), there are 14 lines in the high-field region and 14 lines in the low-field region. More specifically, there are four sets of seven lines, two sets of seven lines for the ^{107}Ag nuclei, and two sets of seven lines for the ^{109}Ag nuclei. Applying the EPR selection rules ($\Delta M_S = \pm 1$, $\Delta m_I = 0$) gives 2I + 1 for the number of hyperfine lines from an interacting nucleus. Thus, the seven hyperfine lines in each set in Fig. 1(b) are a direct result of the I = 3 nuclear spin of the ^{10}B nuclei, whereas the four lines in each set in Fig. 1(a) are the result of the I = 3/2 nuclear spin of the ^{11}B nuclei. In Fig. 1(b), all 14 lines in the two sets are resolved in the high-field region, while only nine lines are resolved in the low-field region because of the strong overlap of the inner lines. The unambiguous identification of ^{11}B and ^{10}B as the participating nuclei in the spectra in Fig. 1 allows us to now refer to the responsible defect as Center Ag–B. This label indicates that the Ag interstitial ion is sharing the unpaired spin with a B ion at a regular lattice position.

The following spin Hamiltonian describes the EPR spectra in Fig. 1. An electron Zeeman term is included along with hyperfine terms for the Ag and B nuclei,

$$H = \beta \mathbf{S} \cdot \mathbf{g} \cdot \mathbf{B} + \mathbf{I}^{\mathbf{Ag}} \cdot \mathbf{A}_{\mathbf{Ag}} \cdot \mathbf{S} + \mathbf{I}^{\mathbf{B}} \cdot \mathbf{A}_{\mathbf{B}} \cdot \mathbf{S}. \quad (1)$$

The spectra in Fig. 1 have little angular dependence and, thus, can be explained with isotropic matrices (i.e., one g value and one A value for each isotope). Numerical values for these parameters are obtained from the [001] data. Treating the **g** and **A** matrices as isotropic allows us to reduce the spin Hamiltonian in Eq. (1) to a simpler form in Eq. (2), with only three parameters. The magnetic field direction is z and raising and lowering operators are introduced,

$$H = g\beta B S_z + A_{Ag} I_z^{Ag} S_z + A_B I_z^B S_z + \frac{1}{2} A_{Ag} \left(I_+^{Ag} S_- + I_-^{Ag} S_+ \right) + \frac{1}{2} A_B \left(I_+^B S_- + I_-^B S_+ \right). \quad (2)$$

When determining values for the parameters, the ^{107}Ag and ^{109}Ag portions of the experimental spectra are considered separately. In Fig. 1(a), ^{11}B is the dominant boron isotope and the spin Hamiltonian for the ^{109}Ag portion of the spectrum is expressed as a 16 × 16 matrix (S = 1/2, I^{Ag} = 1/2, and I^B = 3/2). A best-fit set of values for g, A(^{109}Ag), and A(^{11}B) are obtained from a least-squares fitting program that repeatedly diagonalizes the Hamiltonian matrix (to obtain the energy eigenvalues and, thus, transition energies). The three parameters are systematically varied until the predicted line positions agree with the measured positions. Input data are the microwave frequency and the magnetic field values for individual lines. This same process was followed for the ^{107}Ag portion of the spectrum in Fig. 1(a). A similar procedure was then repeated for the spectrum in Fig. 1(b), where ^{10}B is the dominant boron isotope. In this case, the spin Hamiltonian for each Ag isotope is expressed as a 28 × 28 matrix (S = 1/2, I^{Ag} = 1/2, and I^B = 3). The EPR parameters for Center Ag–B, obtained from fitting the two spectra in Fig. 1, are given in Table II. These results are consistent with those initially reported in Ref. 10.

A more detailed examination of the EPR spectrum from Center Ag–B provides insight into its electronic structure. As indicated earlier, hyperfine splittings from the ^{107}Ag and ^{109}Ag nuclei have no measurable angular dependence, but a small change in the separations of the lines from the ^{11}B nuclei in Fig. 1(a) can be detected when the direction of the magnetic field is sequentially oriented along the three crystal axes. Specifically, at room temperature, the spacings between adjacent ^{11}B hyperfine lines in the

TABLE II. Spin-Hamiltonian parameters for three radiation-induced trapped-electron centers in Ag-doped $Li_2B_4O_7$ crystals. These parameters were obtained from spectra taken with the magnetic field along the [001] direction in the crystal. The spectrum for Center Ag–B was taken at 40 K and the spectra for Center Ag–Ag and Center Ag–Li were taken at room temperature. Units for the hyperfine parameters are MHz. Estimated uncertainties are ±0.0003 for the *g* values and ±2 MHz for the *A* values.

Center Ag–B	Center Ag–Ag	Center Ag–Li
g = 1.9932	g = 1.9820	g = 1.9892
A(^{107}Ag) = 771.8	A_1(^{107}Ag) = 590.0	A(^{107}Ag) = 1384.5
A(^{109}Ag) = 889.7	A_1(^{109}Ag) = 678.3	A(^{109}Ag) = 1592.4
A(^{10}B) = 37.3	A_2(^{107}Ag) = 584.0	A(^{7}Li) = 16.5
A(^{11}B) = 111.2	A_2(^{109}Ag) = 671.3	…

high-field portion of the spectrum are 3.05, 3.05, and 3.65 mT when the magnetic field is along the [100], [010], and [001] directions, respectively. This nearly isotropic ^{11}B matrix, when combined with the isotropic Ag splitting, makes it difficult to extract meaningful information about the directions of the principal axes from a detailed angular study (where data are taken every few degrees when rotating the direction of the magnetic field in three orthogonal planes). Instead, we use the differences in the ^{11}B spacings for the field along the three crystal axes to make an estimate of the unpaired spin density in the 2p orbital on the boron ion.

For an axial interaction, the three principal values of the ^{11}B hyperfine matrix can be expressed as $a-b$, $a-b$, and $a+2b$, where a is the isotropic Fermi contact parameter and b is the anisotropic dipole–dipole parameter.[37] An approximate value for parameter b is one-third of the difference between the largest and smallest ^{11}B hyperfine spacings reported in the previous paragraph (second-order effects are ignored). This gives $b = 0.20$ mT (or, equivalently, 5.605 MHz). Fitzpatrick *et al.*[38] predict that a B 2p orbital (100% occupied) has a value of $b = 53.24$ MHz for a ^{11}B nucleus (i.e., 2/5 of 133.10 MHz). Here, 2/5 is the angular factor for p orbitals.[39] A comparison of these experimental and predicted values indicates that approximately 10.5% of the unpaired spin density of Center Ag–B is in a 2p orbital at the neighboring B site. Similarly, the average of the three ^{11}B hyperfine spacings in the previous paragraph gives $a = 3.25$ mT (or, equivalently, 91.08 MHz) for the Fermi contact parameter. Fitzpatrick *et al.*[38] predict that a B 2s orbital (100% occupied) has $a = 2312.23$ MHz for a ^{11}B nucleus. A comparison of these experimental and predicted values shows that 3.9% of the unpaired spin density is in a 2s orbital at the neighboring B site.

An estimate for the portion of the unpaired spin density on the Ag ion in Center Ag–B is obtained from the ^{107}Ag hyperfine results in Table II. Since the Ag hyperfine interaction is isotropic, the value of 771.8 MHz represents the Fermi contact parameter. Morton and Preston[39] predict that a Ag 5s orbital (100% occupied) has a value of $a = 1831$ MHz. Following the suggestion by Fitzpatrick *et al.*[38] that the Morton and Preston values are consistently high by about 20%, we reduce the predicted value to 1526 MHz. Comparing the measured value of 771.8 MHz with this predicted value indicates that approximately 50.6% of the unpaired spin density for Center Ag–B is in a 5s orbital on the Ag ion. Together, our estimates of the spin densities in the 2s and 2p orbitals on the B ion and the 5s orbital on the Ag ion account for 65.0% of an unpaired electron. We expect that much of the remaining spin density is on the oxygen ions adjacent to the primary boron ion. This latter spin density will not produce observable hyperfine lines in the EPR spectra as ^{17}O, the one stable oxygen isotope with a nonzero nuclear magnetic moment, is only 0.038% abundant.

Finally, we use a simple electrostatics argument to assign the B interaction in Center Ag–B to a B1 ion (i.e., a boron ion with three oxygen neighbors). A B2 ion with four adjacent negatively charged oxygen ions would repel the trapped electron more than a B1 ion with only three adjacent negatively charged oxygen ions. Also, Islam *et al.*[40] and Santos *et al.*[23] have shown that the conduction band minimum in $Li_2B_4O_7$ is dominated by contributions from B1 ions. Structurally, the B1 ions form nearly planar BO_3 units with (1) sp^2 bonds joining the B ion and the three O ions and (2) a nonbonding 2p orbital extending outward from the plane that contains the four ions. We envision the ground state of Center Ag–B having its unpaired spin localized, in large part, in a hybridized bond involving the 5s state of the Ag interstitial and the 2p state extending out from the plane of the trigonal BO_3 unit. Our distribution of the unpaired spin density among the Ag, the B, and the three neighboring O ions gives a realistic view of the electronic structure of Center Ag–B.

B. Silver–silver trapped electron (Center Ag–Ag)

The second Ag-interstitial trapped-electron center involves two adjacent Ag ions (we refer to the paramagnetic form of this defect as Center Ag–Ag). Its EPR spectrum was reported, but not explained, in earlier studies.[3,10] In the 40 K spectrum shown in Fig. 7 of Ref. 10, there are three sets of unidentified lines near 317, 340, and 363 mT. We have isolated this spectrum in our present study and show that its unique hyperfine pattern is due to nearly equal interactions of the unpaired spin with two Ag nuclei located next to each other.

A three-step process allowed us to obtain a "clean" EPR spectrum for Center Ag–Ag. The $Li_2B_4O_7$ crystal that had been doped with Ag during growth was used. First, the crystal was irradiated at room temperature with x rays. The EPR spectrum in Fig. 2(a) was then taken at room temperature with the magnetic field along the [001] direction. This spectrum in Fig. 2(a) is dominated by the 16-line spectrum of Center Ag–B, but also has less intense lines from Center Ag–Ag that are discernable in the high and middle field regions. Next, the irradiated crystal was held at 93 °C for 20 h while being exposed to room light. After this combined heating and bleaching step, the spectrum in Fig. 2(b) was taken at room temperature. During the exposure to light while being held above room temperature, the intensity of the spectrum from Center Ag–Ag increased while the intensity of the 16-line spectrum from Center Ag–B stayed about the same (see Sec. IV). The spectrum in Fig. 2(c) was generated by subtracting the spectrum in Fig. 2(a) from the spectrum in Fig. 2(b). Center Ag–B is eliminated and only Center Ag–Ag is left in Fig. 2(c).

The EPR spectrum of Center Ag–Ag in Fig. 2(c) has $S = 1/2$ and its hyperfine pattern is easily explained by having the unpaired spin interact nearly equally with two Ag nuclei. These nuclei, at two distinct sites, are labeled Ag_1 and Ag_2. Because of the two isotopes of Ag, there are three distinguishable combinations of the two isotopes and two sites that contribute to the observed spectrum: they are (i) $^{107}Ag_1$ and $^{107}Ag_2$, (ii) $^{107}Ag_1$ and $^{109}Ag_2$ or $^{109}Ag_1$ and $^{107}Ag_2$, and (iii) $^{109}Ag_1$ and $^{109}Ag_2$. The two combinations, $^{107}Ag_1$ and $^{109}Ag_2$ and $^{109}Ag_1$ and $^{107}Ag_2$, are very similar, only distinguished by the slight broadening of their middle lines. Stick diagrams below the spectrum in Fig. 2(c) represent these three distinct combinations. The upper stick diagram is the sum of the three lower stick diagrams and, thus, should be directly compared to the experimental spectrum.

The parameters describing Center Ag–Ag are obtained from its EPR spectrum by using the following spin Hamiltonian:

$$\mathrm{H} = \beta \mathbf{S} \cdot \mathbf{g} \cdot \mathbf{B} + \mathbf{I}^{\mathrm{Ag},1} \cdot \mathbf{A}_{\mathrm{Ag},1} \cdot \mathbf{S} + \mathbf{I}^{\mathrm{Ag},2} \cdot \mathbf{A}_{\mathrm{Ag},2} \cdot \mathbf{S}. \quad (3)$$

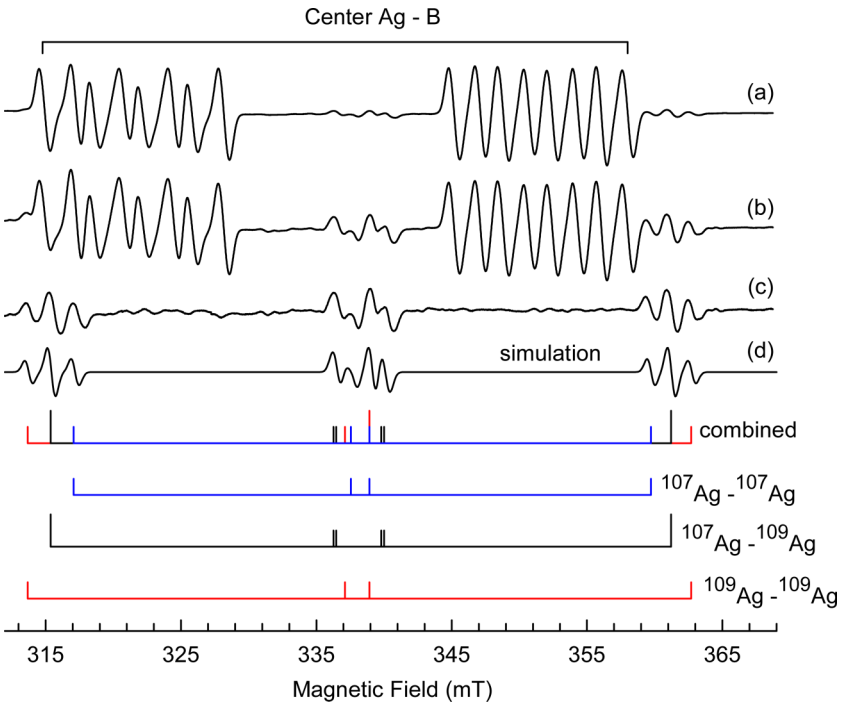

FIG. 2. EPR spectrum from Center Ag–Ag. These data were obtained at room temperature. The magnetic field was along the [001] direction, and the microwave frequency was 9.393 GHz. (a) Spectrum taken after irradiation at room temperature with x rays. (b) Spectrum taken after the irradiated crystal was held at 93 °C for 20 h while being exposed to room light. (c) Difference spectra (trace a subtracted from trace b) showing Center Ag–Ag without interference from Center Ag–B. (d) Simulation of the EPR spectrum from Center Ag–Ag using the parameters in Table II. Stick diagrams below the spectra identify the participating nuclei.

As was the case for Center Ag–B, the spectrum of Center Ag–Ag has little angular dependence. The **g** and **A** matrices are again treated as isotropic, and the spin Hamiltonian is reduced to the simpler form in Eq. (4), with only three parameters,

$$H = g\beta BS_z + A_1 I_z^{Ag,1} S_z + A_2 I_z^{Ag,2} S_z + \frac{1}{2} A_1 \left(I_+^{Ag,1} S_- + I_-^{Ag,1} S_+ \right) + \frac{1}{2} A_2 \left(I_+^{Ag,2} S_- + I_-^{Ag,2} S_+ \right). \quad (4)$$

This spin Hamiltonian is expressed as an 8×8 matrix ($S = 1/2$, $I^{Ag,1} = 1/2$, and $I^{Ag,2} = 1/2$) and then repeatedly diagonalized in a least-squares program to determine the best-fit values for g, A_1, and A_2. Input data, taken from the experimental spectrum in Fig. 2(c), are the microwave frequency and magnetic field values for the lines that correspond to the $^{107}Ag_1$ and $^{109}Ag_2$ combination of isotopes and sites (see the next to the lowest set of stick diagrams). Fitting these lines gives values for the g, $^{107}Ag_1$, and $^{109}Ag_2$ parameters. Then, the $^{107}Ag_2$ and $^{109}Ag_1$ parameters are determined by using the ratio of the ^{107}Ag and ^{109}Ag nuclear magnetic moments (these moments are provided in Table I). The final set of spin-Hamiltonian parameters for Center Ag–Ag is given in Table II. A simulation of the EPR spectrum, generated using Bruker's SimFonia program, is shown in Fig. 2(d). As described in Sec. III A, an unpaired spin in a 5s orbital is predicted to have an isotropic hyperfine interaction of 1526 MHz for the ^{107}Ag isotope.[38,39] Our values of 590 and 587 MHz for $A_1(^{107}Ag)$ and $A_2(^{107}Ag)$, when combined, indicate that about 77.1% of the unpaired spin in Center Ag–Ag is in 5s orbitals on the two Ag ions. The remainder of the unpaired spin may be in the p orbitals on the two Ag ions and, perhaps, in the s and p orbitals on nearby boron and oxygen ions.

Our proposed model for Center Ag–Ag has one of the two Ag ions at an interstitial site. If the two Ag ions in this defect were on adjacent Li^+ sites, they would not be expected to equally share the unpaired spin since they are too far apart. The closest separation of two Li^+ sites in this crystal is approximately 3.08 Å, whereas the separation of the two atoms in a Ag_2 diatomic molecule is 2.53 Å.[41] This suggests that the best way to achieve the nearly equal sharing of the unpaired spin in Center Ag–Ag is to have one Ag ion at an interstitial site and the other Ag ion at the nearest Li^+ site. The greater the separation distance, the more likely there would be an unequal sharing of the unpaired spin between the two Ag ions. We also note that two B^{3+} ion sites are closer to a Li^+ site than the closest neighboring Li^+ site. If the Ag ions were at neighboring Li^+ sites, the unpaired spin would be expected to reside primarily on one of the Ag ions with significantly resolved ^{11}B hyperfine from one or more boron neighbors. The EPR signal from Center Ag–Ag, involving two Ag nuclei and having no resolved ^{11}B hyperfine, directly supports our interstitial model.

C. Silver-lithium trapped electron (Center Ag–Li)

The third trapped-electron center in our $Li_2B_4O_7$ crystals has a large hyperfine interaction with one Ag ion and a much weaker hyperfine interaction with an adjacent ion with an $I = 3/2$ nucleus. Its EPR spectrum, shown in Fig. 3, was taken at room temperature from the crystal doped with Ag during growth. A complex sequence of irradiation, heating, and bleaching, described in the next paragraph, was needed to produce this spectrum. There are

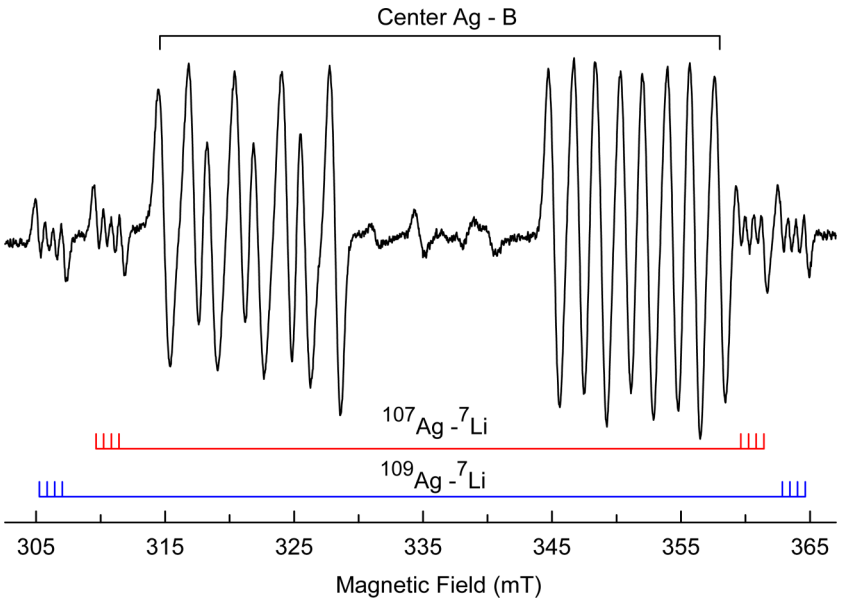

FIG. 3. EPR spectrum from Center Ag–Li. The spectrum was taken at room temperature, with the magnetic field along the [001] direction and a 9.393 GHz microwave frequency. Stick diagrams below the spectrum identify the lines associated with the ^{107}Ag and ^{109}Ag isotopes in the low- and high-field regions.

16 lines in this new EPR spectrum, as illustrated by the stick diagrams in Fig. 3. Each of the four lines from the ^{109}Ag and ^{107}Ag nuclei is further split into four lines by the I = 3/2 nucleus. The resulting groups of closely spaced lines are located near 306.1, 310.5, 360.5, and 363.7 mT (i.e., below and above the 16 lines from Center Ag–B). Since our third EPR spectrum is also seen in the ^{10}B enriched crystal with no change in the hyperfine spacings, we can eliminate ^{11}B as the responsible I = 3/2 nucleus. This leaves ^{7}Li as the only isotope with I = 3/2 that is present in sufficient concentration to account for the observed hyperfine. Thus, the paramagnetic form of this third defect is labeled Center Ag–Li. The EPR spectrum from Center Ag–Li has not been previously reported.

Prior to acquiring the spectrum in Fig. 3, the crystal was irradiated at room temperature with x rays, then warmed to 175 °C and held there for 2 min, and finally exposed to 442 nm laser light after returning to room temperature. The EPR lines from Center Ag–Li were not present after the initial x-ray irradiation, but appeared during the thermal anneal at 175 °C. This anneal significantly reduced the intensity of the set of 16 lines from Center Ag–B. The 442 nm laser light further reduced the intensity of the 16-line spectrum from Center Ag–B, while not affecting the intensity of the lines from Center Ag–Li. We reported in our earlier OSL study[3] that exposure to light near 400 nm reduces the intensity of Center Ag–B. At the present time, the physical mechanisms involved in the multi-step process that produced Center Ag–Li are not identified.

The spin-Hamiltonian parameters describing Center Ag–Li were obtained from the EPR spectrum in Fig. 3. Again, because of very little angular dependence, only three parameters are needed. The spin Hamiltonians in Eqs. (1) and (2) were used, with ^{11}B being replaced with ^{7}Li. This results in a 16 × 16 matrix (S = 1/2, I^{Ag} = 1/2, and I^{Li} = 3/2) that is used in the fitting process. For ^{107}Ag, the input data are the microwave frequency and the magnetic field values for the two sets of four lines near 310.5 and 360.5 mT. For ^{109}Ag, the two sets of four lines near 306.1 and 363.7 mT are used as input data. The final set of spin-Hamiltonian parameters [g, A(^{107}Ag), A(^{109}Ag), and A(^{7}Li)] for Center Ag–Li is given in Table II. Our value of 1384 MHz for A(^{107}Ag) in Table II, when compared to the predicted value of 1526 MHz,[38,39] indicates that 90.7% of the unpaired spin in Center Ag–Li is in a 5s orbital on the interstitial Ag ion.

IV. THERMAL STABILITIES OF THE TRAPPED ELECTRONS

Decay temperatures for the three Ag-related electron traps described in Sec. III were determined in a series of step anneals. The $Li_2B_4O_7$ crystal doped with Ag during growth was initially irradiated at room temperature with x rays, and an EPR spectrum was taken at 60 K. Data points at 22 °C in Fig. 4 represent the relative concentrations of the traps after the irradiation at room temperature. For the first anneal step, the crystal was heated to 75 °C (i.e., the initial T_{stop} value) in the TL reader. As soon as T_{stop} was reached, the heating element was turned off and the sample quickly cooled to room temperature in less than 10 s. The crystal was returned to the EPR spectrometer and a spectrum was again recorded at 60 K. This process was repeated with the T_{stop} value increasing in 25 °C steps, from 75 to 200 °C. An EPR spectrum was taken at 60 K after each heating step.

Figure 4 shows the changing intensities of the three trapped-electron EPR signals during the thermal anneals. After the room temperature irradiation with x rays, the relative concentrations of Center Ag–B and Center Ag–Ag are in the ratio of 20:1. The intensity of the spectrum from Center Ag–B increases between room temperature and 75 °C. This is followed by a slight decrease between 75 and 100 °C, a rapid decrease between 100 and 150 °C, and a slight decrease between 150 and 175 °C. The initial increase of Center Ag–B at 75 °C is attributed to the release of electrons from singly ionized oxygen vacancies[3,24] and their subsequent

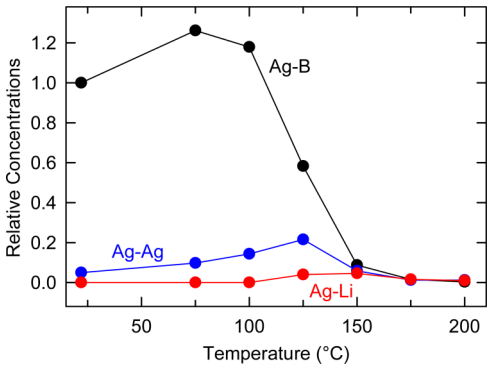

FIG. 4. Thermal decay of the EPR spectra from Centers Ag–B, Ag–Ag, and Ag–Li. The intensities of the EPR spectra (representing their relative concentrations) were monitored at 60 K after an initial irradiation at room temperature with x rays, and then after each step of the heating sequence.

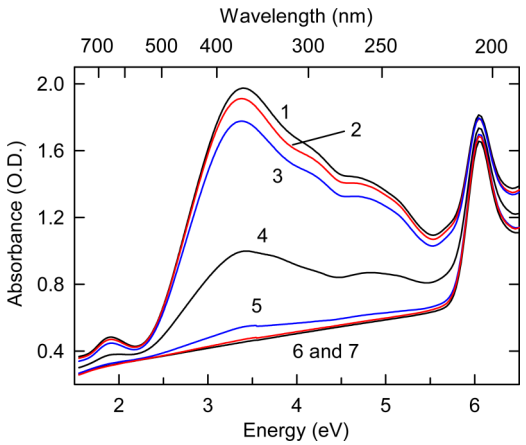

FIG. 5. Optical absorption spectra taken at room temperature from an x-ray-irradiated Ag-doped $Li_2B_4O_7$ crystal. Spectrum 7 was taken before the irradiation and spectrum 1 was taken after after the irradiation. Spectra 2, 3, 4, 5, and 6 were taken after heating to 75, 100, 125, 150, and 175 °C, respectively. The optical path length was 0.8 mm.

trapping at interstitial Ag^+ ions. The intensity of the spectrum from Center Ag–Ag increases between room temperature and 125 °C. This spectrum is roughly four times more intense after heating to 125 °C, with most of the increase attributed to the thermal release of electrons from Center Ag–B and their retrapping to form Center Ag–Ag. The EPR spectrum from Center Ag–Li is not observed until after the 125 °C anneal step. Its intensity increases between 125 and 150 °C and then decreases between 150 and 175 °C. Our results in Fig. 4 show that the three Ag-related trapped electrons have slightly different thermal stabilities, with Center Ag–B being the least stable and Center Ag–Li being the most stable.

V. OPTICAL ABSORPTION

Broad overlapping optical absorption bands appear between 225 and 750 nm when the Ag-doped $Li_2B_4O_7$ crystals are irradiated at room temperature with x rays.[3,15] Figure 5 shows absorption spectra from the crystal that was doped with Ag during growth. These spectra, taken before and after irradiation and then after each step of a series of thermal anneals of the irradiated crystal, were obtained at room temperature with unpolarized spectrometer light propagating along the [001] direction. In the spectrum taken before the irradiation (curve 7), the only feature present is the intense absorption band peaking near 205 nm (6.05 eV). It represents the $4d^{10}$ to $4d^95s^1$ transition of the Ag^+ ions at Li^+ sites.[3,11,13,17] This Ag^+ band decreases significantly in intensity, but does not disappear during the irradiation. As seen in Fig. 5, new absorption produced by the radiation appears in the same short wavelength region (i.e., under the 205 nm band). An intense absorption band peaking near 370 nm (3.35 eV) dominates the spectrum (curve 1) taken after the irradiation. Two additional less intense and only slightly resolved absorption bands near 297 nm (4.17 eV) and 254 nm (4.88 eV) are on the high-energy side of the primary 370 nm band. The weak band peaking near 660 nm (1.88 eV) has also been produced by the radiation. In Fig. 5, the surface plasmon resonance of small Ag nanoparticles within the crystal may be responsible for the "background" absorption that increases toward shorter wavelengths with a λ^{-1} dependence.[42]

The detailed analysis by Santos *et al.*[23] shows that the entirety of the induced absorption in curve 1 of Fig. 5, from 500 to 250 nm, can be attributed to $5s \rightarrow 5p$ and $4d \rightarrow 5s$ transitions of Ag^0 atoms (i.e., Ag-related trapped-electron centers) and that the band near 660 nm is due to $d \rightarrow d$ transitions of Ag^{2+} ions (i.e., Ag-related trapped hole centers). Specifically, the band at 370 nm is assigned to the electric-dipole-allowed $4d^{10}5s^1$ to $4d^{10}5p^1$ transition of the Ag^0 centers. The $4d^{10}5p^1$ excited state participating in this transition is predicted to be close to the conduction band minimum, thus allowing thermally assisted photoionization to occur at room temperature.[3,23] In an earlier experimental study,[3] exposing a crystal to 400 nm light released electrons from the Ag^0 centers and produced a strong OSL response. In the present study, we reaffirm this photoionization mechanism by observing a rapid drop in the concentration of Ag^0 electron traps when an x-ray-irradiated Ag-doped $Li_2B_4O_7$ crystal is illuminated at room temperature with 405 nm laser light (i.e., the EPR signals and optical absorption bands from the Ag^0 centers both decrease when pumping into the broad 370 nm absorption band).

Curves 2, 3, 4, 5, and 6 in Fig. 5 were taken after heating to 75, 100, 125, 150, and 175 °C, respectively. From a comparison of Figs. 4 and 5, it is clear that the thermal decay of the 370 nm absorption band correlates with the thermal decay of the EPR spectrum from Center Ag–B. Both the optical absorption at 370 nm and the EPR signal from Center Ag–B have large decreases between 100 and 150 °C.

VI. THERMOLUMINESCENCE

Electrons thermally released from their Ag-related trapping sites recombine with holes at Ag^{2+} centers[14,16] and produce a

thermoluminescence (TL) peak near 150 °C with emission peaking at 270 nm. Numerous studies have reported this TL peak in the Ag-doped $Li_2B_4O_7$ crystals.[1,2,10,13,14] To demonstrate that the TL peak correlates with the Ag-related electron traps (Centers Ag–B, Ag–Ag, and Ag–Li), we monitored the residual TL after each step of a series of thermal anneals (similar to the anneal steps described in Figs. 4 and 5 in Secs. IV and V). The crystal was initially irradiated with x rays at room temperature and then heated to 75 °C, the first T_{stop} temperature. After rapidly returning to room temperature, the residual TL from 50 to 225 °C was obtained. The crystal was irradiated again at room temperature, heated to the next higher T_{stop} value, returned to room temperature, and the residual TL curve taken. These residual TL glow curves are shown in Fig. 6. The largest decrease in the intensity of the residual TL occurs between 125 and 150 °C.

The step annealing experiments described in Sec. IV show that the three Ag-related electron traps have slightly different thermal stabilities. This, in turn, suggests that the main TL response near 150 °C in the Ag-doped $Li_2B_4O_7$ crystals consists of three closely spaced TL peaks that reflect the different thermal stabilities of the electron traps. There could, of course, be more than three contributing peaks. As demonstrated by Coleman and Yukihara,[43] the initial rise method for analyzing TL data is not expected to resolve these overlapping peaks. The primary contribution to the observed TL glow curve is the thermal release of electrons from Center Ag–B. The release of electrons from the two additional traps (Center Ag–Ag and Center Ag–Li) with their slightly greater thermal stabilities, but reduced concentrations, results in a lingering tail to the main TL peak.

The participation of three similar electron traps presents a challenge when modeling the TL response of the Ag-doped $Li_2B_4O_7$ crystals. Assuming a linear superposition of three TL curves may not be sufficient since the electron traps are not independent of each other. Detrapping and retrapping processes must be considered, as well as dose-dependent effects. Also, samples with differing concentrations of Ag ions, oxygen vacancies, and lithium vacancies may have distinguishable TL responses. An increase in the Ag dopant level, for example, is expected to shift the TL glow peak to a higher temperature (near 160 °C). This is because the Ag–Ag centers, with their higher thermal stability (see Fig. 4), will be a much greater percentage of the electron traps produced during the irradiation.

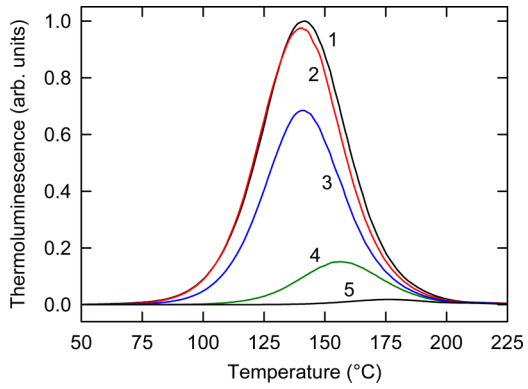

FIG. 6. Residual thermoluminescence peaks obtained by heating a Ag-doped $Li_2B_4O_7$ crystal from 50 to 225 °C at a rate of 1 °C/s. Before taking each TL curve, the crystal was irradiated at room temperature with x rays, heated to the T_{stop} temperature, and then returned to room temperature. The T_{stop} temperatures for curves 1, 2, 3, 4, and 5 were 75, 100, 125, 150, and 175 °C, respectively.

VII. SUMMARY

When Ag-doped $Li_2B_4O_7$ crystals are exposed at room temperature to ionizing radiation, electrons are trapped at interstitial Ag ions. Three distinct $S = 1/2$ electron paramagnetic resonance (EPR) spectra are observed, each involving an interstitial Ag ion sharing the unpaired spin with a neighboring ion at a regular lattice site. Using a ^{10}B enriched crystal, the dominant trap is shown to be an interstitial Ag ion interacting with a B ion at a regular lattice site (referred to as Center Ag–B). A second trap has the interstitial Ag ion interacting with a Ag ion substituting for a Li ion (referred to as Center Ag–Ag). The third trap has the interstitial Ag ion interacting with a Li ion at a regular lattice site (referred to as Center Ag–Li). Radiation-induced optical absorption bands in the 250–500 nm region are assigned to $5s \rightarrow 5p$ and $4d \rightarrow 5s$ transitions of the three trapped-electron centers. The thermal decay of the EPR spectra and their related optical absorption bands coincide with the TL response of the crystals.

ACKNOWLEDGMENTS

T.D.G. was supported by the Air Force Institute of Technology by a National Research Council (NRC) research assistantship. The views expressed in this paper are those of the authors and do not necessarily reflect the official policy or position of the Air Force, the Department of Defense, or the United States Government.

AUTHOR DECLARATIONS

Conflict of Interest

The authors have no conflicts to disclose.

DATA AVAILABILITY

The data that support the findings of this study are available within the article.

REFERENCES

[1]G. D. Patra, S. G. Singh, A. K. Singh, M. Tyagi, D. G. Desai, B. Tiwari, S. Sen, and S. C. Gadkari, "Silver doped lithium tetraborate ($Li_2B_4O_7$) single crystals as efficient dosimeter material with sub-micro-Gy sensitivity," J. Lumin. **157**, 333 (2015).

[2]G. D. Patra, S. G. Singh, B. Tiwari, A. K. Singh, D. G. Desai, M. Tyagi, S. Sen, and S. C. Gadkari, "Optically stimulated luminescence in Ag doped $Li_2B_4O_7$ single crystal and its sensitivity to neutron detection and dosimetry in OSL mode," Radiat. Meas. **88**, 14 (2016).

[3]B. E. Kananen, E. S. Maniego, E. M. Golden, N. C. Giles, J. W. McClory, V. T. Adamiv, Y. V. Burak, and L. E. Halliburton, "Optically stimulated luminescence (OSL) from Ag-doped $Li_2B_4O_7$ crystals," J. Lumin. **177**, 190 (2016).

[4]R. Hemam, L. R. Singh, A. I. Prasad, P. Gogoi, M. Kumar, M. P. Chougaonkar, S. D. Singh, and R. N. Sharan, "Critical view on TL/OSL properties of $Li_2B_4O_7$ nanoparticles doped with Cu, Ag and co-doping Cu, Ag: Dose response study," Radiat. Meas. **95**, 44 (2016).
[5]A. Ozdemir, V. Altunal, V. Guckan, N. Can, K. Kurt, I. Yegingil, and Z. Yegingil, "Characterization and some fundamental features of optically stimulated luminescence measurements of silver activated lithium tetraborate," J. Lumin. **202**, 136 (2018).
[6]R. Chen and S. W. S. McKeever, *Theory of Thermoluminescence and Related Phenomena* (World Scientific Publishing Company, 1997).
[7]E. G. Yukihara and S. W. S. McKeever, *Optically Stimulated Luminescence: Fundamentals and Applications* (John Wiley and Sons, Chichester, 2011).
[8]*Advances in Physics and Applications of Optically and Thermally Stimulated Luminescence*, edited by R. Chen and V. Pagonis (World Scientific Publishing Company, Singapore, 2019).
[9]B. T. Huy, V. X. Quang, and H. T. B. Chau, "Effect of doping on the luminescence properties of $Li_2B_4O_7$," J. Lumin. **128**, 1601 (2008).
[10]A. T. Brant, B. E. Kananan, M. K. Murari, J. W. McClory, J. C. Petrosky, V. T. Adamiv, Y. V. Burak, P. A. Dowben, and L. E. Halliburton, "Electron and hole traps in Ag-doped lithium tetraborate ($Li_2B_4O_7$) crystals," J. Appl. Phys. **110**, 093719 (2011).
[11]G. D. Patra, M. Tyagi, D. G. Desai, B. Tiwari, S. Sen, and S. C. Gadkari, "Photoluminescence properties of Cu and Ag doped $Li_2B_4O_7$ single crystals at low temperatures," J. Lumin. **132**, 1101 (2012).
[12]M. Ignatovych, M. Fasoli, and A. Kelemen, "Thermoluminescence study of Cu, Ag and Mn doped lithium tetraborate single crystals and glasses," Radiat. Phys. Chem. **81**, 1528 (2012).
[13]G. D. Patra, S. G. Singh, B. Tiwari, S. Sen, D. G. Desai, and S. C. Gadkari, "Thermally stimulated luminescence process in copper and silver co-doped lithium tetraborate single crystals and its implication to dosimetry," J. Lumin. **137**, 28 (2013).
[14]D. A. Buchanan, M. S. Holston, A. T. Brant, J. W. McClory, V. T. Adamiv, Y. V. Burak, and L. E. Halliburton, "Electron paramagnetic resonance and thermoluminescence study of Ag^{2+} ions in $Li_2B_4O_7$ crystals," J. Phys. Chem. Solids **75**, 1347 (2014).
[15]A. T. Brant, D. A. Buchanan, J. W. McClory, V. T. Adamiv, Y. V. Burak, L. E. Halliburton, and N. C. Giles, "Photoluminescence from Ag^{2+} ions in lithium tetraborate ($Li_2B_4O_7$) crystals," J. Lumin. **153**, 79 (2014).
[16]I. Romet, E. Aleksanyan, M. G. Brik, G. Corradi, A. Kotlov, V. Nagirnyi, and K. Polgár, "Recombination luminescence of Cu and/or Ag doped lithium tetraborate single crystals," J. Lumin. **177**, 9 (2016).
[17]N. S. Rawat, M. S. Kulkarni, M. Tyagi, P. Ratna, D. R. Mishra, S. G. Singh, B. Tiwari, A. Soni, S. C. Gadkari, and S. K. Gupta, "TL and OSL studies on lithium borate single crystals doped with Cu and Ag," J. Lumin. **132**, 1969 (2012).
[18]O. Annalakshmi, M. T. Jose, U. Madhusoodanan, B. Venkatraman, and G. Amarendra, "Kinetic parameters of lithium tetraborate based TL materials," J. Lumin. **141**, 60 (2013).
[19]Y. S. Horowitz, I. Eliyahu, and L. Oster, "Kinetic simulations of thermoluminescence dose response: Long overdue confrontation with the effects of ionization density," Radiat. Prot. Dosim. **172**, 524 (2016).
[20]D. Kurali, E. Ekdal Karali, A. Kelemen, V. Holovey, N. Can, and T. Karali, "Thermoluminescence characterization of Ag-doped $Li_2B_4O_7$ single crystal materials," Luminescence **32**, 786 (2017).
[21]M. G. Celik, A. Yilmaz, and A. N. Yazici, "Synthesis and thermoluminescence characterization of lithium tetraborate ($Li_2B_4O_7$) doped with copper and silver metals," Radiat. Meas. **102**, 16 (2017).
[22]J. F. Benavente, J. M. Gómez-Ros, and V. Correcher, "Characterization of the thermoluminescence glow curve of $Li_2B_4O_7$:Cu,Ag," Radiat. Meas. **137**, 106427 (2020).
[23]C. Santos, A. F. Lima, and M. V. Lalic, "Structural, electronic and optical characterization of substitutional Ag defect in $Li_2B_4O_7$ scintillator," J. Phys. Chem. Solids. **146**, 109615 (2020).
[24]M. W. Swinney, J. W. McClory, J. C. Petrosky, S. Yang, A. T. Brant, V. T. Adamiv, Y. V. Burak, P. A. Dowben, and L. E. Halliburton, "Identification of electron and hole traps in lithium tetraborate ($Li_2B_4O_7$) crystals: Oxygen vacancies and lithium vacancies," J. Appl. Phys. **107**, 113715 (2010).
[25]J. Krogh-Moe, "Crystal structure of lithium diborate, $Li_2O.2B_2O_3$," Acta Crystallogr. **15**, 190 (1962).
[26]N. Sennova, R. Bubnova, J. Shepelev, S. Filatov, and O. Yakovleva, "$Li_2b_4O_7$ crystal structure in anharmonic approximation at 20, 200, 400 and 500(C)," J. Alloys Compd. **428**, 290 (2007).
[27]N. Sennova, R. S. Bubnova, G. Cordier, B. Albert, S. K. Filatov, and L. Isaenko, "Temperature-dependent changes of the crystal structure of $Li_2B_4O_7$," Z. Anorg. Allg. Chem. **634**, 2601 (2008).
[28]V. T. Adamiv, Y. V. Burak, and I. M. Teslyuk, "The crystal structure of $Li_2B_4O_7$ compound in the temperature range 10–290 K," J. Alloys Compd. **475**, 869 (2009).
[29]K. Momma and F. Izumi, "VESTA 3 for three-dimensional visualization of crystal, volumetric and morphology data," J. Appl. Crystallogr. **44**, 1272 (2011).
[30]See https://jp-minerals.org/vesta/en/ for VESTA software.
[31]R. D. Shannon, "Revised effective ionic radii and systematic studies of interatomic distances in halides and chalcogenides," Acta Crystallogr. A **32**, 751 (1976).
[32]J.-M. Spaeth and H. Overhof, *Point Defects in Semiconductors and Insulators: Determination of Atomic and Electronic Structure from Paramagnetic Hyperfine Interactions* (Springer-Verlag, Berlin, 2003).
[33]N. J. Stone, "Table of nuclear magnetic dipole and electric quadrupole moments," At. Data Nucl. Data Tables **90**, 75 (2005).
[34]M. Berglund and M. E. Wieser, "Isotopic compositions of the elements 2009 (IUPAC technical report)," Pure Appl. Chem. **83**, 397 (2011).
[35]G. Mitrikas, C. C. Trapalis, and G. Kordas, "Electron spin-lattice relaxation of silver nanoparticles embedded in SiO_2 and TiO_2 matrices," J. Chem. Phys. **111**, 8098 (1999).
[36]M. Danilczuk, A. Lund, J. Sadlo, H. Yamada, and J. Michalik, "Conduction electron spin resonance of small silver particles," Spectrochim. Acta A **63**, 189 (2006).
[37]J.-M. Spaeth, J. R. Niklas, and R. H. Bartram, *Structural Analysis of Point Defects in Solids: An Introduction to Multiple Magnetic Resonance Spectroscopy* (Springer-Verlag, Berlin, 1992), pp. 53–56.
[38]J. A. J. Fitzpatrick, F. R. Manby, and C. M. Western, "The interpretation of molecular magnetic hyperfine interactions," J. Chem. Phys. **122**, 084312 (2005).
[39]J. R. Morton and K. F. Preston, "Atomic parameters for paramagnetic resonance data," J. Magn. Res. (1969) **30**, 577 (1978).
[40]M. M. Islam, V. V. Maslyuk, T. Bredow, and C. Minot, "Structural and electronic properties of $Li_2B_4O_7$," J. Phys. Chem. B **109**, 13597 (2005).
[41]B. Simard, P. A. Hackett, A. M. James, and P. R. R. Langridge-Smith, "The bond length of silver dimer," Chem. Phys. Lett. **186**, 415 (1991).
[42]I. I. Kindrat, B. V. Padlyak, R. Lisiecki, A. Drzewiecki, and V. T. Adamiv, "Effect of silver co-doping on luminescence of the Pr^{3+}-doped lithium tetraborate glass," J. Lumin. **241**, 118468 (2022).
[43]A. C. Coleman and E. G. Yukihara, "On the validity and accuracy of the initial rise method investigated using realistically simulated thermoluminescence curves," Radiat. Meas. **117**, 70 (2018).